

# Quantum Spin Liquid in Spin 1/2 $J_1$ - $J_2$ Heisenberg Model on Square Lattice: Many-Variable Variational Monte Carlo Study Combined with Quantum-Number Projections

Satoshi Morita<sup>1\*</sup>, Ryui Kaneko<sup>2</sup>, and Masatoshi Imada<sup>3</sup>

<sup>1</sup>*Institute for Solid State Physics, University of Tokyo, Kashiwa, Chiba 277-8581, Japan*

<sup>2</sup>*Institute für Theoretische Physik, Goethe-Universität Frankfurt, Max-von-Laue-Straße 1, 60438 Frankfurt am Main, Germany*

<sup>3</sup>*Department of Applied Physics, University of Tokyo, Bunkyo, Tokyo 113-8656, Japan*

Nature of quantum spin liquids is studied for the spin-1/2 antiferromagnetic Heisenberg model on the square lattice containing exchange interactions between the nearest-neighbor sites,  $J_1$  and those between the next-nearest-neighbor sites,  $J_2$ . We perform variational Monte Carlo simulations combining with quantum-number-projection technique and clarify the phase diagram in the ground state together with its excitation spectra. We obtain the non-magnetic phase in the region  $0.4 < J_2/J_1 \leq 0.6$  sandwiched by the staggered and stripe antiferromagnetic (AF) phases. Our direct calculations of the spin gap support that the triplet excitation from the singlet ground state is gapless in the region  $0.4 < J_2/J_1 \leq 0.5$ , while the gapped valence-bond-crystal (VBC) phase is stabilized for  $0.5 < J_2/J_1 \leq 0.6$ . The VBC order is likely to have the columnar symmetry with the spontaneous symmetry breaking of the  $C_{4v}$  symmetry. The power-law behaviors of the spin-spin and dimer-dimer correlation functions in the gapless region are consistent with the emergence of the algebraic quantum-spin-liquid phase (critical phase). The exponent of the spin correlation  $\langle S(0)S(r) \rangle \propto 1/r^{z+\eta}$  at a long distance  $r$  appears to increase from  $z + \eta \sim 1$  at  $J_2/J_1 \sim 0.4$  toward the continuous transition to the VBC phase at  $J_2/J_1 \sim 0.5$ . Our results, however, do not fully exclude the possibility of a direct quantum transition between the staggered AF and VBC phase with a wide critical region and deconfined criticality.

---

\*E-mail: morita@issp.u-tokyo.ac.jp

## 1. Introduction

In the presence of strong geometrical frustration and quantum fluctuations, insulators without any long range order, the quantum spin liquid (SL) states, may appear even at zero temperature. One of the simplest models proposed for the quantum spin liquid state is a spin 1/2 antiferromagnetic  $J_1$ - $J_2$  Heisenberg model on the square lattice (Fig. 1). The variables  $J_1$  and  $J_2$  denote the nearest- and next-nearest-neighbor interactions, respectively. In the small  $J_2$  region, just as in the Heisenberg model on the square lattice, the ground state is believed to have the staggered antiferromagnetic (AF) long-ranged order with a Bragg peak at  $\mathbf{q} = (\pi, \pi)$  in the spin structure factor. On the other hand, when  $J_2$  becomes comparable to  $J_1$ , the stripe AF long-ranged order with the Bragg peaks at  $\mathbf{q} = (0, \pi)$  and  $(\pi, 0)$  in the spin structure factor is stabilized. In the intermediate region,  $J_2 \sim J_1/2$ , geometrical frustration and quantum fluctuations have been proposed to suppress the long-range magnetic and valence-bond-crystal (VBC) orders.<sup>1-9</sup>

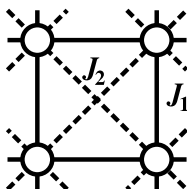


**Fig. 1.** Lattice structure of the antiferromagnetic  $J_1$ - $J_2$  Heisenberg model on the square lattice. At  $J_2 = 0$ , the structure is the simple square lattice. We use the periodic-periodic boundary condition.

There are several high-precision numerical methods to obtain ground states of strongly correlated electron systems. Among others, the variational Monte Carlo (VMC) method based on the fermionic resonating-valence-bond (RVB) state is a powerful tool to examine the quantum spin liquid states. More recently, Hu *et al.* investigated the  $J_1$ - $J_2$  Heisenberg model using the VMC method with the Lanczos technique and reported that the energy gap between the ground state and the triplet excited state with the total momentum  $\mathbf{K} = (\pi, 0)$  closes in the region  $0.48 \leq J_2/J_1 \leq 0.6$ .<sup>6</sup>

The density matrix renormalization group (DMRG) method is one of the highly accurate numerical techniques. It is originally developed in one-dimensional electron systems and recently applied to two-dimensional ones with the cylindrical boundary condition. Jiang *et al.* have revisited the ground-state properties of the  $J_1$ - $J_2$  Heisenberg model by using DMRG.<sup>7</sup> They have reported a spin-gapped quantum spin liquid phase

in the region  $0.41 \leq J_2/J_1 \leq 0.62$ . The quantum spin liquid state is characterized by the absence of the long-ranged magnetic and dimer orders. Contrary to these results, Gong *et al.* showed a gapless region without any magnetic and VBC orders for  $0.44 < J_2/J_1 < 0.5$  using DMRG with  $SU(2)$  spin rotation symmetry.<sup>8</sup>

In various numerical results, the intermediate region  $0.4 \lesssim J_2/J_1 \lesssim 0.6$  has been interpreted as the spin liquid phase with either gapless<sup>4,6,8</sup> or gapful<sup>5,7,9</sup> triplet excitations, while it has alternatively been interpreted by the deconfinement criticality, where a novel quantum criticality dominated by the deconfinement of magnons emerges at the critical point between the AF and stripe AF (or VBC) phases. In this proposal, the spin liquid phase does not exist in the ground state but only the critical point exists while the parameters away from the critical point belong always in either of the ordered phases in the strict sense.

It has also been proposed that the intermediate phase contains VBC phases including the columnar order<sup>1,2,10–12</sup> and the plaquette order.<sup>3,13,14</sup> By using DMRG, Gong *et al.*<sup>8</sup> have reported that a plaquette VBC phase appears for  $0.5 < J_2/J_1 < 0.61$ .

Although both the VMC and DMRG methods predict the quantum spin liquid state in the intermediate region of the  $J_1$ - $J_2$  Heisenberg model, nature of this state such as the spin gap is controversial. Among all, very recent state-of-the-art studies, one by VMC<sup>6</sup> and the other two by DMRG<sup>7,8</sup> have reached conclusions contradicting each other, in terms of the phase diagram and the spin liquid properties. The nature and the existence itself of the quantum spin liquid phase are, therefore, still under hot debate.

One possible reason for the discrepancy is the bias inevitably exists in the VMC methods. As is the case of the calculation by Hu *et al.*, the variational wave functions are often assumed to have a certain symmetry through the mean-field Hamiltonian.<sup>6</sup> Another possible origin of the discrepancy could be insufficient number of states kept in the DMRG studies. The limitation of tractable number of states also constrains the lattice shape to cylindrical geometry, and the maximum size of the circumference, at most 12 or 14 sites.

To elucidate the origin of the discrepancy, in particular, between the VMC and DMRG results, we perform VMC simulations by using improved variational wave functions that can reproduce both spin-gapped and spin-gapless states in a unified form. We employ the many-variable variational Monte Carlo (mVMC) method<sup>15</sup> to the model of the square size  $L \times L$  with the periodic boundary condition, which is more symmetric than the cylindrical boundary condition studied by the DMRG method and makes

the extrapolation to the thermodynamic limit easier. To reduce biases of the variational wave functions, we introduce generalized one body part of the variational wave functions so that they can compare both spin-gapped and spin-gapless states on equal footing. To obtain singlet and triplet excited states, we apply several quantum-number projections to specify the quantum numbers of the wavefunction such as the total spin and momentum, which must be preserved because they commute with the Hamiltonian. This procedure not only enables higher accuracy but also allows us to calculate the energy gaps and the excitation spectra directly.

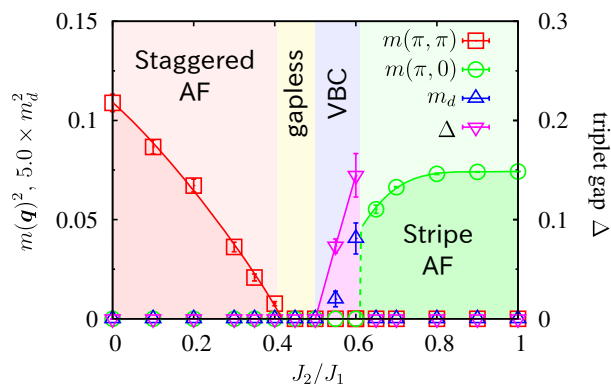


**Fig. 2.** (Color online) Ground-state phase diagram of  $J_1$ - $J_2$  Heisenberg model on square lattice obtained in the present study. Staggered (stripe) magnetizations are denoted by  $m(\mathbf{q})$  with  $\mathbf{q} = (\pi, \pi)$  ( $\mathbf{q} = (\pi, 0)$ ). The dimer order parameter  $m_d$  is multiplied by 5.0 and  $\Delta$  denotes the triplet spin gap. The curves are guide for the eyes. For the definitions of  $m(\mathbf{q})$  and  $m_d$ , see Sec. 3.

Our calculations up to  $16 \times 16$  sites yield the ground-state phase diagram after the size extrapolation to the thermodynamic limit as shown in Fig. 2. The staggered (stripe) AF phase exist for  $J_2/J_1 \leq 0.4$  ( $J_2 > 0.6$ ) and the ground state for  $0.4 < J_2/J_1 \leq 0.6$  has no magnetic order. In this non-magnetic region, we found that the triplet gap closes and becomes gapless in the region  $0.4 < J_2/J_1 \leq 0.5$ , while the VBC phase is obtained for  $0.5 < J_2/J_1 \leq 0.6$  with gapful spin-triplet excitations. We also report the power-law decay of the spin-spin correlation function in the gapless region indicating the existence of an algebraic spin-liquid phase in an extended region.

This paper is organized as follows. In Sec. 2, we first introduce the  $J_1$ - $J_2$  Heisenberg model and the mVMC method with quantum-number projections. In Sec. 3, we determine the quantum numbers of the ground state and excited states and report results of order parameters and the triplet gap. The nature of the non-magnetic region and the properties of phase transition points are discussed in Sec. 4. Section 5 is devoted to the

conclusions.

## 2. Model and method

We consider the spin 1/2 antiferromagnetic  $J_1$ - $J_2$  Heisenberg model on the square lattice. The Hamiltonian is given by

$$H = J_1 \sum_{\langle i,j \rangle} \mathbf{S}_i \cdot \mathbf{S}_j + J_2 \sum_{\langle\langle i,j \rangle\rangle} \mathbf{S}_i \cdot \mathbf{S}_j, \quad (1)$$

where  $\langle i,j \rangle$  and  $\langle\langle i,j \rangle\rangle$  denote nearest-neighbor and next-nearest-neighbor sites, respectively;  $\mathbf{S}_i$  is the spin 1/2 operator on site  $i$ . In the following, we set  $J_1 = 1$  as a unit of energy. We calculate the ground state and low-energy excited states of the model under the periodic boundary conditions.

To obtain physical properties of the states, we use the mVMC method with quantum-number projections.<sup>15</sup> We employ a fermionic representation of the trial wave functions of the form given by

$$|\psi\rangle = \mathcal{P}_G \mathcal{L} |\phi_{\text{pair}}\rangle, \quad (2)$$

where  $|\phi_{\text{pair}}\rangle$  and  $\mathcal{L}$  denote the one-body part and the quantum number projection, as we detail later. The Gutzwiller projection,

$$\mathcal{P}_G = \prod_i (1 - n_{i\uparrow} n_{i\downarrow}), \quad (3)$$

prohibits the double occupation of the electron.

The one body part is given by a generalized pair wave function defined as

$$|\phi_{\text{pair}}\rangle = \left( \sum_{i,j} f_{ij} c_{i\uparrow}^\dagger c_{j\downarrow}^\dagger \right)^{N_s/2} |0\rangle, \quad (4)$$

where  $c_{i\sigma}^\dagger$  ( $c_{i\sigma}$ ) denotes the creation (annihilation) operator of electrons on the site  $i$  with spin  $\sigma$ , and  $N_s = L^2$  is the number of sites. The pairing amplitude  $f_{ij}$  is taken as variational parameters depending on  $i, j$  and determined by optimization. This pair wave function can describe antiferromagnetic, VBC as well as spin liquid states on equal footing. In itinerant systems, in addition to the above variety of Mott insulators, it can describe metals, and superconductors as well. A long-range pairing amplitude is necessary to represent a state with spin correlations decaying with a power law as a function of distance.

In the conventional VMC calculations based on the RVB states, we first derive the mean-field BCS Hamiltonian, and then optimize the order parameters such as the

magnetization and superconducting gap. The pairing amplitude of the one body part are determined by these order parameters. Although this approach is simple and intuitive, the wave functions remains primitive and biased. To reduce such biases, instead, we directly optimize the pairing amplitude.

In principle, it is better to use a flexible trial wave function without any constraint on  $f_{ij}$ . We however assume  $2 \times 2$  sublattice structure of  $f_{ij}$  by assuming the translational invariance in terms of this sublattice period in order to reduce computational costs. Namely, we impose the constraint  $f_{ij} = f_{kl}$  if  $\mathbf{r}_i - \mathbf{r}_k = \mathbf{r}_j - \mathbf{r}_l = (2n, 2m)$  for arbitrary integers  $n$  and  $m$ , where  $\mathbf{r}_i$  is the spatial coordinate of the site  $i$ . Therefore the number of independent variational parameters for  $f_{ij}$  is  $4N_s$ . This sublattice structure is suitable for potential candidates of the ground state of this model such as staggered and stripe AF orders as well as for the VBC orders. We confirm that  $2 \times 2$  sublattice structure is sufficient and larger ones change our results little. In fact, this constraint itself is justified unless the ground state has the long-range order with the period longer than the size of the sublattice. Meanwhile, we do not impose any constraint between  $f_{ij}$  and  $f_{ji}$ .

An inner product between the pair wave function and a real-space electron configuration is represented by a Pfaffian of a skew-symmetric matrix. To calculate Pfaffian, we employ the PFAPACK library<sup>16</sup> and fast update technique described in Appendix.

Naive optimizations do not preserve the inherent symmetries of the finite system. To restore the symmetries, we take into account quantum-number projections, which have successfully been used in the path-integral renormalization group method<sup>17</sup> and the Gaussian-basis Monte Carlo method.<sup>18</sup> In this study, we use the spin quantum-number projection, the total momentum projection, and the lattice symmetry projection:

$$\mathcal{L} = \mathcal{L}_S \mathcal{L}_K \mathcal{L}_L. \quad (5)$$

We note that the quantum number projection is commutative with the Gutzwiller projection. The spin quantum number projection  $\mathcal{L}_S$  restores the  $SU(2)$  spin-rotational symmetry by superposing wave functions rotated in the spin space.<sup>15</sup>

The total momentum projection  $\mathcal{L}_K$  and the lattice symmetry projection  $\mathcal{L}_L$  restore the translational symmetry and the point group symmetry of lattice, respectively. The former is defined as

$$\mathcal{L}_K \equiv \frac{1}{N_s} \sum_{\mathbf{R}} e^{-i\mathbf{K} \cdot \mathbf{R}} T_{\mathbf{R}}, \quad (6)$$

where  $T_{\mathbf{R}}$  is a translational operator to shift all the spatial coordinates by  $\mathbf{R}$ . The  $2 \times 2$  sublattice structure of  $f_{ij}$  restricts the total momentum to  $\mathbf{K} = (0, 0)$ ,  $(0, \pi)$ ,  $(\pi, 0)$ , or  $(\pi, \pi)$ . The point group of the square lattice is  $C_{4v}$  composed of a  $\pi/2$  rotation and a reflection along the vertical axis. When the total momentum is  $\mathbf{K} = (0, \pi)$  or  $(\pi, 0)$ , the wave function has the symmetry of  $C_{2v}$ . The lattice symmetry projection to an irreducible representation  $\beta$  is represented as

$$\mathcal{L}_{\mathbf{L}}^{(\beta)} = \frac{d_{\beta}}{g} \sum_R \chi_R^{(\beta)} R, \quad (7)$$

where  $d_{\beta}$  and  $g$  are the dimension of the irreducible representation and the number of elements  $R$  in the point group, respectively. The characters  $\chi_R^{(\beta)}$  of  $C_{4v}$  and  $C_{2v}$  are listed in Table I. Here,  $C_4$  is a  $\pi/2$  rotation and  $C_2 = C_4^2$ . A reflection along the vertical axis and the diagonal line is denoted by  $\sigma_v$  and  $\sigma_d$ , respectively. For  $C_{2v}$ ,  $\sigma_x$  is a reflection along  $x$  axis and  $\sigma_y = \sigma_x C_2$ .

**Table I.** The character tables of  $C_{4v}$  and  $C_{2v}$

$C_{4v}$	$E$	$2C_4$	$C_2$	$2\sigma_v$	$2\sigma_d$
$A_1$	1	1	1	1	1
$A_2$	1	1	1	-1	-1
$B_1$	1	-1	1	1	-1
$B_2$	1	-1	1	-1	1
$E$	2	0	-2	0	0

$C_{2v}$	$E$	$C_2$	$\sigma_y$	$\sigma_x$
$A_1$	1	1	1	1
$A_2$	1	1	-1	-1
$B_1$	1	-1	1	-1
$B_2$	1	-1	-1	1

A large number of the variational parameters are optimized according to the stochastic reconfiguration method developed by Sorella.<sup>19</sup> After confirming the energy convergence, we calculate the expectation values of the physical quantities and average them over 10 independent runs to estimate statistical errors.

### 3. Results

We first investigate magnetic property of the ground state to determine the phase diagram. The spin structure factors, defined as

$$S(\mathbf{q}) = \frac{1}{N_s} \sum_{i,j} e^{i\mathbf{q} \cdot (\mathbf{r}_i - \mathbf{r}_j)} \langle \mathbf{S}_i \cdot \mathbf{S}_j \rangle, \quad (8)$$

are shown in Fig. 3. For small  $J_2$ , the spin structure factor has a sharp peak at  $\mathbf{q} = (\pi, \pi)$  corresponding to the staggered AF state, while it has two sharp peaks at  $\mathbf{q} = (\pi, 0)$  and  $(0, \pi)$  for large  $J_2$  corresponding to the stripe AF state. For the intermediate  $J_2$ , a suppressed peak appears at  $\mathbf{q} = (\pi, \pi)$ , which signals a nonmagnetic state. We emphasize that our trial wave function can represent both magnetic-ordered states because of the direct optimization of the pairing amplitude.

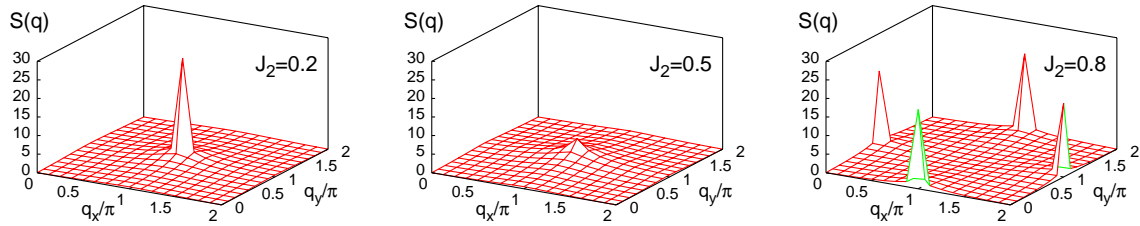


**Fig. 3.** (Color online) Static spin structure factors  $S(\mathbf{q})$  for  $16 \times 16$  lattice system at  $J_2/J_1 = 0.2$ ,  $0.5$ , and  $0.8$ .

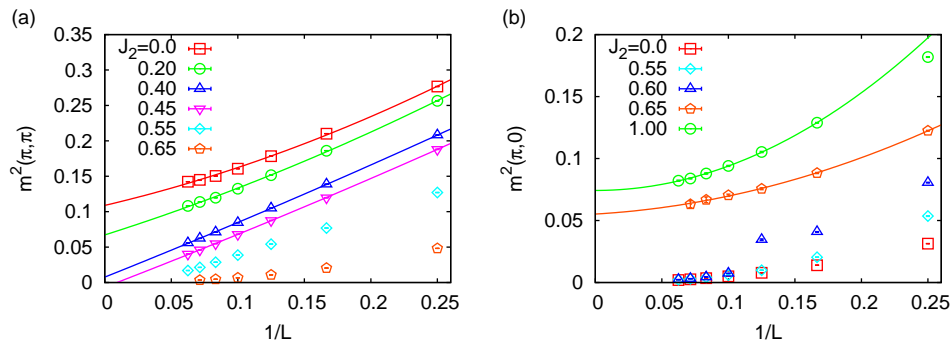


**Fig. 4.** (Color online) Finite-size extrapolation of square magnetizations. (a) Staggered AF order parameters with AF wave vector  $(\pi, \pi)$ , and (b) Stripe AF order parameters with  $(\pi, 0)$  are fitted by square polynomials of  $1/L$ .

To analyze the existence of magnetic long-range order, we extrapolate the magnetic order parameter  $m(\mathbf{q})^2 = S(\mathbf{q})/N_s$  by fitting with square polynomials of  $1/L$  as shown in



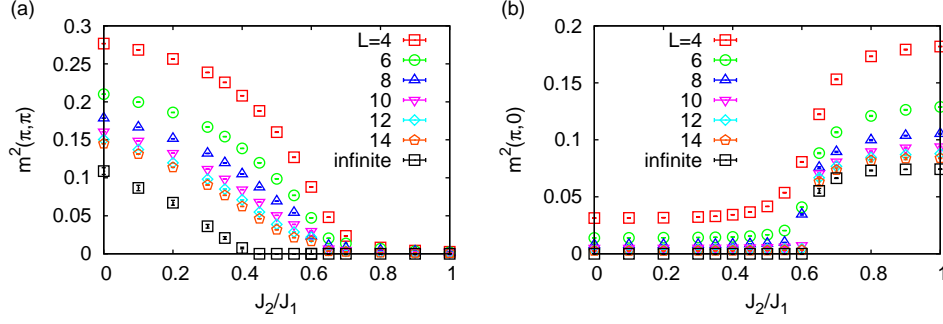


**Fig. 5.** (Color online) (a) Staggered and (b) stripe AF order parameters as a function of  $J_2/J_1$  plotted for various calculated sizes with their extrapolations to thermodynamic limit.

Fig. 4. Note that the spin-wave approximation shows the finite-size correction in power of  $1/L$ .<sup>20</sup> Finite-size extrapolation shows that the staggered and stripe AF orders are nonzero for  $J_2 \leq 0.4$  and  $J_2 > 0.6$ , respectively (Fig. 5). Therefore, we conclude that the staggered and stripe AF phases exist for  $J_2 \leq 0.4$  and  $J_2 > 0.6$ , respectively (Fig. 2). The intermediate region ( $0.4 < J_2 \leq 0.6$ ) has no magnetic order. The phase boundary and values of magnetization are in agreement with previous studies.

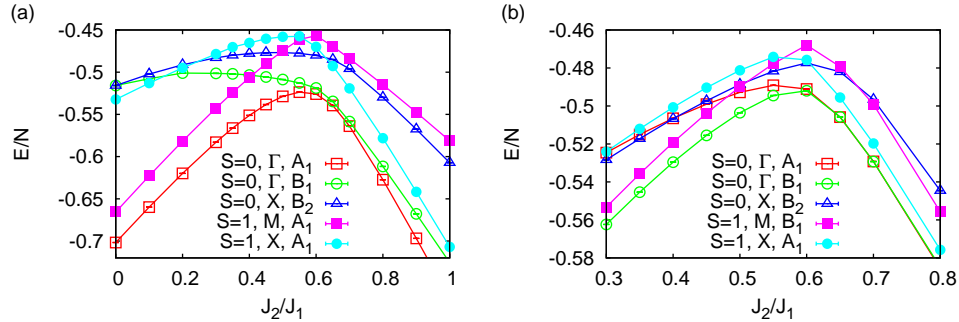


**Fig. 6.** (Color online) Ground-state and excited-state energies for (a)  $L = 4$  and (b)  $L = 6$  as functions of  $J_2$ .  $A_i$  and  $B_i$  ( $i = 1$  or  $2$ ) are irreducible representations of the point group  $C_{4v}$  for  $\Gamma$  ( $\mathbf{K} = (0,0)$ ) and  $M$  ( $\mathbf{K} = (\pi, \pi)$ ) points and ones of  $C_{2v}$  for  $X$  point ( $\mathbf{K} = (\pi, 0)$ ).

The quantum numbers of the ground state are determined by calculating the lowest energy with every combination of total spin ( $S = 0$  or  $1$ ), total momentum and lattice symmetry. In Figs. 6 and 7, we show the lowest energy with given quantum numbers.

The ground state always has total momentum  $\mathbf{K} = (0,0)$  and total spin  $S = 0$ , and the even parity under the reflection along the vertical axis. The parity of  $\pi/2$  lattice rotation, however, depends on the system size. The ground state of  $L = 4n$  has the

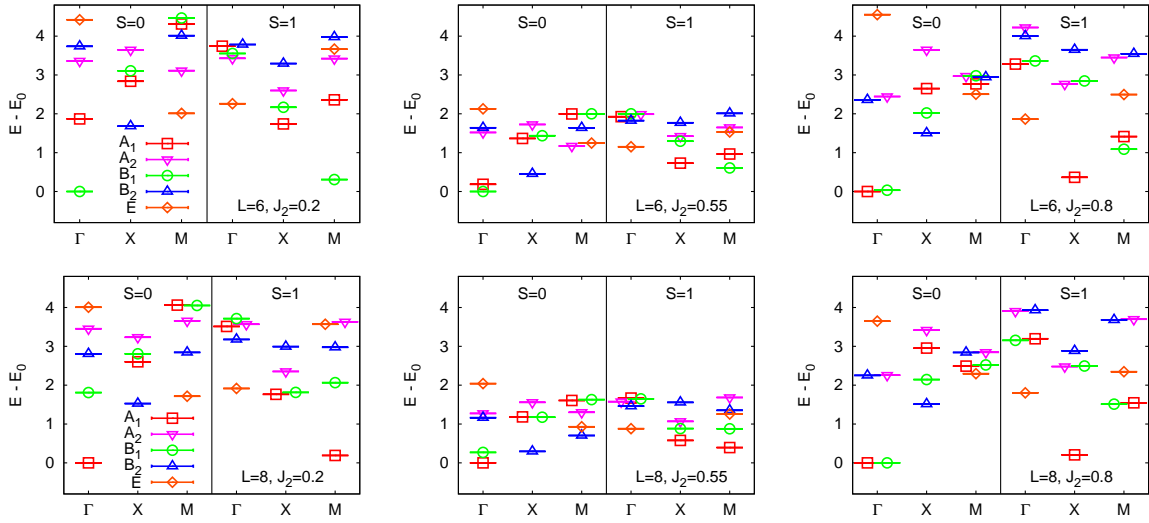


**Fig. 7.** (Color online) The lowest excitation energy with given quantum numbers for  $L = 6$  and  $L = 8$  with  $J = 0.2, 0.55$  and  $0.8$ . The symbols denote irreducible representations of the point group  $C_{4v}$  for  $\Gamma$  ( $\mathbf{K} = (0,0)$ ) and  $M$  ( $\mathbf{K} = (\pi,\pi)$ ) and of  $C_{2v}$  for  $X$  point ( $\mathbf{K} = (\pi,0)$ ).

even parity for all  $J_2$ . On the other hand, for  $L = 4n + 2$ , the energy level crossing occurs at the transition point  $J_2 \sim 0.6$  between the non-magnetic region and the stripe AF phase. The ground state for small (large)  $J_2$  is odd (even) under  $\pi/2$  rotation. For  $J_2 > 0.6$ , the ground state with even parity for  $\pi/2$  rotation and the first singlet excited state with the odd parity eventually degenerate in the thermodynamic limit.

As shown in Fig. 6, the lowest triplet excited states cross at the phase boundary between the staggered AF phase and the non-magnetic region. The first triplet excited state for  $J_2 < 0.6$  has the total momentum  $\mathbf{K} = (\pi,\pi)$ , while the one for  $J_2 > 0.6$  has  $\mathbf{K} = (\pi,0)$  or  $(0,\pi)$ , which corresponds to the staggered and stripe AF wave vectors. The both triplet excited states are even under the reflection along the vertical axis. For  $J_2 < 0.6$ , the lowest triplet excited state has the same parity of  $\pi/2$  rotation as the ground state. Thus in this region, the triplet gap is defined as the energy difference between the singlet state with  $\mathbf{K} = (0,0)$  and the triplet state with  $\mathbf{K} = (\pi,\pi)$ . For  $L = 4n$  ( $4n + 2$ ), the both states belong to the same irreducible representation  $A_1$  ( $B_1$ ) of  $C_{4v}$ . We will discuss in the next section how we should understand the symmetry of the ground state and the excitation spectra.

Next, we investigate the triplet gap to characterize the non-magnetic region for  $0.4 < J_2 \leq 0.6$ . As we previously showed, the lowest triplet state in this region has the total momentum  $\mathbf{K} = (\pi,\pi)$  and belongs to the irreducible representation  $A_1$  ( $B_1$ ) for

$$L = 4n(4n + 2).$$

We consider two kinds of the system-size dependence of the triplet gap:

$$\Delta(N_s) = \Delta_\infty + \frac{a}{N_s} + \frac{b}{N_s^{3/2}}, \quad (9)$$

and

$$\Delta(N_s) = \Delta_\infty + \frac{a'}{N_s^{1/2}} + \frac{b'}{N_s}, \quad (10)$$

where  $\Delta_\infty$  denotes the triplet gap in the thermodynamic limit. The former scaling form consists with a dispersion relation of the triplet excitation,<sup>21,22</sup>

$$\Delta(\mathbf{k}) = \sqrt{\Delta_\infty^2 + v^2(\mathbf{k} - \mathbf{k}_0)^2}, \quad (11)$$

because the non-zero wave-vector scales as  $|\mathbf{k} - \mathbf{k}_0| \sim \pi/L$  in the finite-size system. The spin-wave analysis also yields that the leading order of the triplet gap is scaled by  $1/N_s$  for an antiferromagnetic ordered state in two-dimensional systems.<sup>23,24</sup> Hence, if the gap is nonzero or if the AF order exists, this scaling form is more appropriate. The latter form (10) with  $\Delta_\infty = 0$  is justified at the quantum critical point and in the quantum critical phase with the dynamical critical exponent  $z = 1$ . If we obtain a negative gap  $\Delta_\infty < 0$  by the size extrapolation, we fit parameters again with fixed  $\Delta_\infty = 0$ .

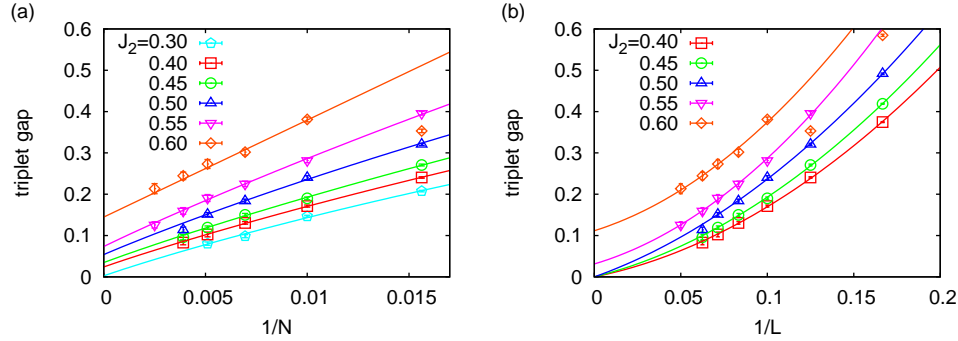


**Fig. 8.** (Color online) Finite-size extrapolation of triplet gap  $\Delta(L)$ . (a) Triplet gaps are plotted as a function of  $1/N$  and fits of the data to the form Eq. (9) are shown as solid curves. (b) Triplet gaps as a function of  $1/L$  are fitted by Eq. (10)

In Fig. 8, we show the spin gap for various system sizes. The data fit well the scaling form (9) in the whole range of  $J_2$  and we obtain the non-zero spin gap in the thermodynamic limit for  $0.4 \leq J_2 \leq 0.6$ . As shown in Fig. 8(b), however the spin gap does not conflict with the scaling form (10) as well for the critical phase for the region

$0.4 \leq J_2 \leq 0.5$ . The triplet gap is concave downward as a function of  $1/N$ , which implies that the scaling form (9) may overestimate the triplet gap in the thermodynamic limit. On the other hand, convex fitting of the triplet gap as a function of  $1/L$  in Fig. 8(a) may cause underestimates. We show below that the triplet excitation is likely to be gapless for  $0.4 \leq J_2 \leq 0.5$  making the scaling form in Fig. 8(b) more appropriate. However, for  $J_2 > 0.5$ , even the scaling form (10) produces a nonzero spin gap. The gapful triplet excitation for  $J_2 > 0.5$  is consistent with the VBC order identified below.

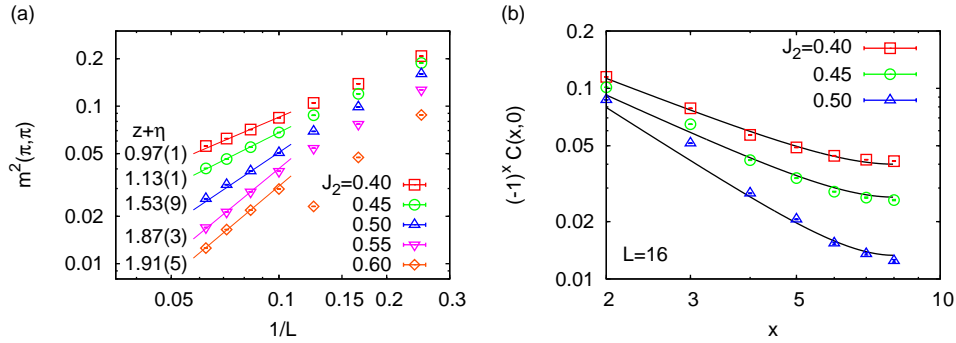


**Fig. 9.** (Color online) (a) Log-log plot of magnetic order parameter. The solid lines are obtained by fitting with  $L^{-(z+\eta)}$ . The uncertainties in the last digits of the numerical data are determined by the fitting and do not take into account possible systematic finite-size effects. (b) Spin-spin correlation functions along  $x$ -axis for  $L = 16$ . The solid lines are Eq. (14) with  $z + \eta$  obtained from the left panel.

To further clarify the criticality of the non-magnetic region,  $0.4 < J_2 \leq 0.5$ , we re-examine the size-dependence of the magnetic order parameter  $m(L)$ . If we assume that the correlation function decays as  $C(r) \propto r^{-(d+z-2+\eta)}$ , the peak value of the structure factor is expected to follow the system-size scaling

$$S(\mathbf{q}_{\text{peak}}, L) \sim \int_{\Lambda}^L dr \frac{r^{d-1}}{r^{d+z-2+\eta}} \propto L^{2-(z+\eta)} \quad (12)$$

with  $\Lambda$  being a cutoff, and then  $m(L)^2 \propto L^{-(z+\eta)}$ . Figure 9(a), which is a log-log plot of the staggered magnetization against the system size, clearly supports the critical behavior in the non-magnetic region, namely for  $0.4 < J_2 \leq 0.5$ . Note that the region  $0.5 < J_2 \leq 0.6$  does not contradict the behavior  $S(\mathbf{q}_{\text{peak}}, L)/N_s \sim \int_0^L dr r^{d-1} \exp[-r/\xi]/N_s \propto 1/L^2$ , indicating the exponential decay of the correlation, because the scaling at  $J_2 = 0.55$  and  $0.6$  in Fig. 9 is close to  $m^2 \propto 1/L^2$  within the uncertainty of the estimate of the exponent arising from the finite-size effect.

We also calculate the spin-spin correlation function defined as

$$C(\mathbf{r}) = \frac{1}{N_s} \sum_{\mathbf{r}'} \langle \mathbf{S}_{\mathbf{r}} \cdot \mathbf{S}_{\mathbf{r}+\mathbf{r}'} \rangle. \quad (13)$$

By considering the effect of the periodic boundary condition, we assume that data fit with the following form:

$$C(\mathbf{r}) \propto \frac{1}{|\mathbf{r}|^{z+\eta}} + \sum_{\mathbf{n} \neq (0,0)} \left( \frac{1}{|\mathbf{r} + L\mathbf{n}|^{z+\eta}} - \frac{1}{|L\mathbf{n}|^{z+\eta}} \right), \quad (14)$$

where  $\mathbf{n} = (n_x, n_y)$  is an integer vector. The power-law decay of the spin-spin correlation function as shown in Fig. 9(b) is consistent with the power-law scaling of the magnetic order parameter.

Therefore we conclude that the non-magnetic phase in  $0.4 < J_2 \leq 0.5$  is critical and gapless and hence the spin gap in this region should be scaled by Eq. (10). We note again that the phase in  $0.5 < J_2 \leq 0.6$  is gapped and the triplet gap should be fit with Eq. (9). The obtained triplet gap in the thermodynamic limit is shown in Fig. 2.

To investigate the possibility of a VBC order, we next consider the dimer structure function defined as

$$S_d(\mathbf{q}) = \frac{1}{N_s} \sum_{i,j} e^{i\mathbf{q} \cdot (\mathbf{r}_i - \mathbf{r}_j)} (\langle B_i^x B_j^x \rangle - \langle B_i^x \rangle \langle B_j^x \rangle), \quad (15)$$

where  $B_i^x$  is a bond operator along  $x$ -axis,  $B_i^x = \mathbf{S}_i \cdot \mathbf{S}_{i+\hat{x}}$ . In the non-magnetic region,  $S_d(\mathbf{q})$  has a peak at  $\mathbf{q}_x = (\pi, 0)$ , which signals an expected columnar or plaquette VBC order. Therefore we consider the dimer order parameter to characterize the VBC phase, defined as  $m_d^2 = S_d(\mathbf{q}_x)/N_s$ .

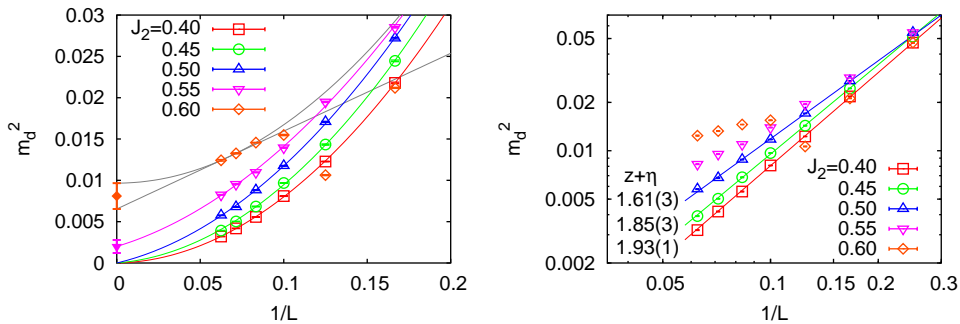


**Fig. 10.** (Color online) Size dependence of dimer order parameters. (a) The data are fitted by  $a + b/L + c/L^2$ . (b) Log-log plot of the same data. The solid lines are obtained by fitting with  $L^{-(z+\eta)}$ .

In Fig. 10, we show size dependences of the dimer order parameter  $m_d^2$ . By fitting  $m_d^2$

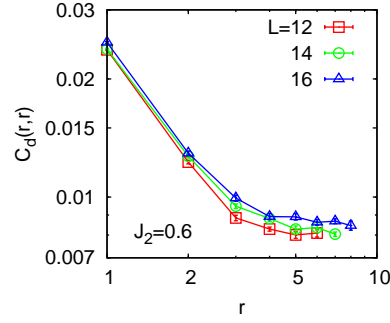


**Fig. 11.** (Color online) The real-space dimer correlation function along the diagonal line ( $x = y$ ) at  $J_2 = 0.6$ .

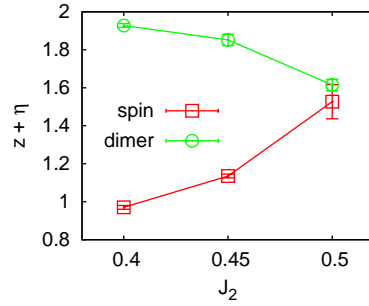


**Fig. 12.** (Color online) Exponent  $z + \eta$  estimated from the staggered AF magnetic order parameter (Fig. 9(a)) and the dimer order parameter (Fig. 10(b)).

with quadratic of  $1/L$  in the same way as the magnetic order parameter, we obtain no VBC order in the gapless region  $J_2 \leq 0.5$ . On the other hand, the gapped non-magnetic phase for  $0.5 < J_2 \leq 0.6$  has a small VBC order. For  $J_2 = 0.6$ , since the finite size effect is strong, we estimate the upper and lower bounds of the extrapolated value of  $m_d^2$  by fitting the last three points from  $L = 12$  to 16 with  $a + c/L^2$  and  $a' + b'/L$ . We note that these three points are convex as a function of  $1/L$ , which implies the finite dimer order parameter in the thermodynamic limit. The real-space dimer correlation function at  $J_2 = 0.6$  is shown in Fig. 11, which is consistent with the long-range ordered state with  $m_d^2 \sim 0.009$  in agreement with Fig. 10(a).

Figure 10(b) shows a log-log plot of the dimer order parameter. We find that the data are fit well with the power-law scaling form  $m_d^2 \propto L^{-(z+\eta_d)}$  in the gapless region  $0.4 < J_2 \leq 0.5$ . For  $J_2 = 0.4$ , the obtained exponents  $z + \eta_d$  are close to two, which is expected in a state without the VBC order where the VBC correlation decays exponentially at long distance. The obtained exponent  $z + \eta$  for the spin correlation and  $z + \eta_d$  for the

dimer correlation are plotted in Fig. 12. It is remarkable that the exponent  $\eta$  appears to vary depending on  $J_2$ .

#### 4. Discussion

We first comment on accuracy of our calculations. In a  $4 \times 4$  system, the trial wave functions (2) reproduce exact energies for both ground and excited states.<sup>1</sup> The calculated variance of energy,  $\langle H^2 \rangle - \langle H \rangle^2$ , is equal to zero, which indicates that obtained states are exact eigenstates of the Hamiltonian. For a  $6 \times 6$  lattice, the ground-state energy per site with  $J_2 = 0.6$  by the mVMC method is  $E/N_s = -0.50355(1)$ , while the one by the exact diagonalization is  $-0.50381$ . The error of the energy is an order of magnitude smaller than the preceding VMC result based on the projected-BCS state.<sup>25</sup> In larger systems, the ground state energy of our calculation is comparable with results obtained after one Lanczos step reported in Ref. 6.

We determined the quantum numbers of the ground state and excited states by using the projection technique. In the region  $J_2 < 0.4$ , the results in Figs. 6 and 7 are consistent with the expectation that the lowest-energy triplet state with  $\mathbf{K} = (\pi, \pi)$  becomes degenerate with the ground state in the thermodynamic limit as it should be in the staggered AF order. On the other hand, in the region  $J_2 > 0.6$ , the results are consistent with the expectation that the lowest-energy triplet states with  $\mathbf{K} = (\pi, 0)$  and  $(0, \pi)$  together with the ground state become degenerate as it should be in the stripe AF order.

In the non-magnetic region, the lowest excitation energy with each quantum number is smaller than the staggered and stripe AF phase (7). This implies that strong geometric frustrations destabilize magnetic ordered states.

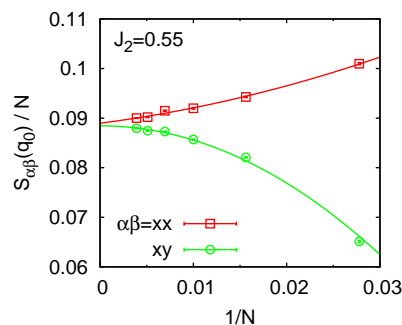


**Fig. 13.** (Color online) The dimer structure factors  $S_{\alpha\beta}(\mathbf{q})$  at  $\mathbf{q}_0 = (0, 0)$  for  $J_2 = 0.55$ . The data are fitted by square polynomials of  $1/N$ .

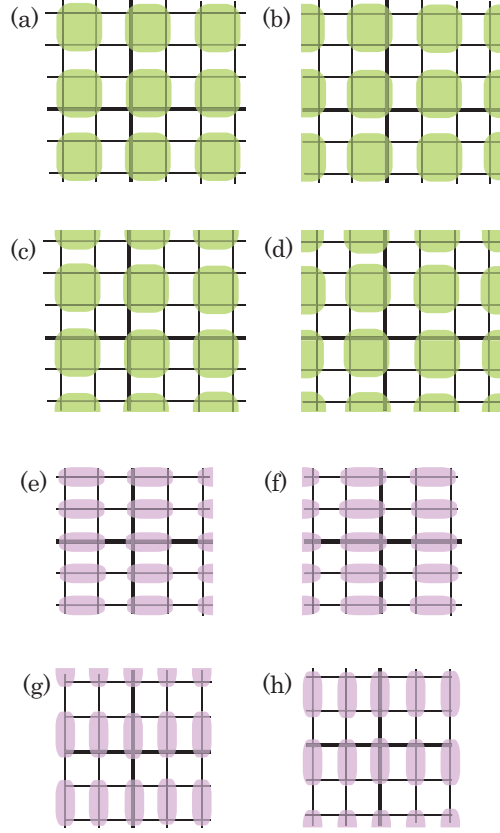


**Fig. 14.** (Color online) (a),(b),(c),(d): Schematic illustration of four-fold degenerate plaquette VBC order. The plaquettes are illustrated by the shaded green area. (e),(f),(g),(h): Four-fold degenerate columnar VBC order. The dimers are illustrated by the shaded purple area.

The criterion to distinguish columnar and plaquette VBC orders was proposed in Ref. 14. They discussed difference of the dimer structure factors at  $\mathbf{q}_0 = (0, 0)$ ,

$$C_{\text{col}} \simeq \frac{1}{N_s^2} \sum_{ij} \langle B_i^x B_j^x - B_i^x B_j^y \rangle = \frac{1}{N_s} (S_{xx}(\mathbf{q}_0) - S_{xy}(\mathbf{q}_0)), \quad (16)$$

$$S_{\alpha\beta}(\mathbf{q}) = \frac{1}{N_s} \sum_{ij} e^{i\mathbf{q} \cdot (\mathbf{r}_i - \mathbf{r}_j)} \langle B_i^\alpha B_j^\beta \rangle, \quad (17)$$

and argued that  $C_{\text{col}}$  took zero for the plaquette VBC order, while non-zero for the columnar VBC order, based on the perfectly-ordered VBC state. As shown in Fig. 13, the VBC phase satisfy the criterion  $C_{\text{col}} \rightarrow 0$  in the thermodynamic limit.

However, this criterion is insufficient to distinguish the two VBC phases. The counter-example of their criterion is found in an imperfect columnar VBC state. Let us assume that, in the state  $|e\rangle$  illustrated in Fig. 14(e), the expectation value of the bond operator satisfies  $B_i^x = b_0$  if the bond  $(i, i + \hat{x})$  is on the shaded dimer, and oth-



erwise  $B_i^x = b_1$ . We also assume that the bond operators perpendicular to dimers have  $B_i^y = b_2$ . The perfectly-ordered VBC state satisfies  $b_1 = b_2 = 0$ . The other states ( $f$ ,  $g$ ,  $h$ ) are generated by the spatial translations and the  $\pi/2$  rotation. The expectation value of  $C_{\text{col}}$  for  $|e + f + g + h\rangle$  becomes zero if  $b_0 + b_1 = 2b_2$  though this state still has the columnar VBC order. Thus the criterion  $C_{\text{col}} \rightarrow 0$  is insufficient to exclude the columnar VBC order.

The extrapolated values of  $S_{\alpha\beta}(\mathbf{q}_0)/N_s$  in Fig. 13 and the dimer order parameter  $m_d$  in Fig. 10 impose restrictions on both the columnar and plaquette VBC order. We note that  $m_d^2 = S_{xx}(\mathbf{q}_x)/N_s$  because of the translational symmetry. For the columnar VBC state with  $b_0 + b_1 = 2b_2$ , we have  $S_{xx}(\mathbf{q}_0)/N_s \rightarrow (b_0 + b_1)^2/4$  and  $m_d^2 \rightarrow (b_0 - b_1)^2/8$ .

On the other hand, for the plaquette VBC state illustrated in Fig. 14(a)-(d), let us assume  $B_i^\alpha = p_0$  if the bond  $(i, i + \hat{\alpha})$  is on the shaded plaquette and otherwise  $B_i^\alpha = p_1$ . Then, we obtain  $S_{xx}(\mathbf{q}_0)/N_s \rightarrow (p_0 + p_1)^2/4$  and  $m_d^2 \rightarrow (p_0 - p_1)^2/4$ . For  $J_2 = 0.55$ , the finite-size extrapolations show  $S_{xx}(\mathbf{q}_0)/N_s = 0.0889(4)$  and  $m_d^2 = 0.0020(7)$  in the thermodynamic limit. Therefore, if the columnar VBC order exists,  $b_0 = 0.36(2)$  and  $b_1 = 0.25(2)$  must be satisfied, while in case of the plaquette VBC order,  $p_0 = 0.34(1)$  and  $p_1 = 0.25(1)$  are required.

**Table II.** The total momentum  $\mathbf{K}$  and the irreducible representation  $\beta$  of the four singlet states for plaquette and columnar VBC order illustrated in Fig. 14

plaquette	$\mathbf{K}$	$\beta$	columnar	$\mathbf{K}$	$\beta$
$a + b + c + d$	$\Gamma (0, 0)$	$A_1$	$e + f + g + h$	$\Gamma (0, 0)$	$A_1$
$a - b + c - d$	$X (\pi, 0)$	$B_2$	$e - f$	$X (\pi, 0)$	$B_2$
$a + b - c - d$	$X' (0, \pi)$	$B_1$	$g - h$	$X' (0, \pi)$	$B_1$
$a - b - c + d$	$M (\pi, \pi)$	$B_2$	$e + f - g - h$	$\Gamma (0, 0)$	$B_1$

Here, we discuss the plausible VBC order pattern from the viewpoint of its excitation. The linear combinations of four states for plaquette VBC order illustrated in Fig. 14(a)-(d) and the columnar VBC order in Fig. 14(e)-(h) can construct four singlets, whose quantum numbers are listed in Table. II. For both of the VBC states, three of the four singlet states have the same symmetries, namely,  $A_1$  on the  $\Gamma$  point,  $B_2$  on the  $X$  point, and  $B_1$  on the  $X'$  point. As shown in Fig. 7, our VBC state well reproduces this degeneracy at  $J_2 = 0.55$ ; the energy of the singlet state with  $B_2$  on the  $X$  point (and the equivalent  $B_1$  on the  $X'$  point) is very close to the ground-state energy at the

$\Gamma$  point with the  $A_1$  symmetry.

The only difference between the plaquette and columnar VBC orders appears in the singlet excitation spectra on the  $\Gamma$  and  $M$  points. If the plaquette VBC order is realized, the singlet state with  $B_2$  irreducible representation on the  $M$  point should be degenerated with the other three states in the thermodynamic limit. However, such a behavior is not observed in the present calculation (Fig. 7). On the other hand, the negligibly small energy gap between singlet states with  $A_1$  and  $B_1$  on the  $\Gamma$  point is compatible with the columnar VBC order.

Although our results for excitation spectra support the columnar VBC phase, results on larger system sizes are desired to decisively conclude whether the singlet state with  $B_2$  on the  $M$  point is degenerate in the thermodynamic limit. The plaquette-plaquette correlation allows to clarify more directly whether the VBC phase in  $0.5 < J_2 \leq 0.6$  is columnar or plaquette. However, since an  $m$ -spin correlation function takes computational costs scaled by at least  $O(m^3)$ , calculations of plaquette-plaquette correlations requiring computations of 8-spin correlations remain a future challenge.

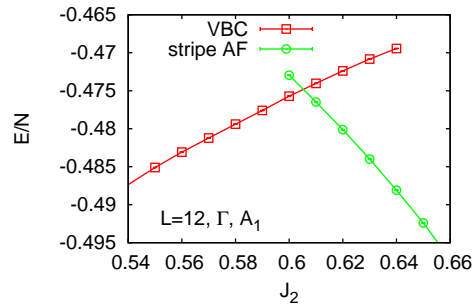


**Fig. 15.** (Color online) The level crossing between the VBC and stripe AF states at the first-order transition point around  $J_2 = 0.6$  for  $12 \times 12$  lattice system. The both states have the total momentum  $\mathbf{K} = (0, 0)$  and the irreducible representation  $A_1$ .

Our data support that the first-order transition occurs between the stripe AF phase and the non-magnetic region around  $J_2 = 0.6$ . As previously shown, the quantum numbers of the lowest triplet state change at this transition point. We also observe that, for  $L = 4n$ , the metastable state with the quantum numbers same as the ground state survive around the transition point as shown Fig. 15.

On the other hand, the phase transition between the staggered AF phase and the non-magnetic region around  $J_2 = 0.4$  is continuous with the critical exponent  $\beta \sim 1/2$

since the square of magnetic order parameter linearly depends on  $J_2$  around the phase boundary (Fig. 5(a)). This behavior is also observed in previous calculations.<sup>7,8</sup> At  $J_2 = 0.4$ , the staggered AF order is close to the critical point and the magnetic order parameter is fit well with the critical scaling form  $L^{-(z+\eta)}$  as shown in Fig. 9. The obtained exponent  $(z+\eta)$  is close to unity. This fact indicates that the phase transition between the staggered AF phase and the non-magnetic phase has very small  $\eta$  with the quantum criticality  $z = 1$  expected from the linear dispersion at the critical point by taking  $\Delta_\infty = 0$  in Eq. (11). Further studies are necessary to understand why the obtained critical exponents are close to the mean-field value. The same characteristic behavior  $z + \eta \sim 1$  is also observed in the  $J_1$ - $J_2$  Heisenberg model on the triangular lattice.<sup>26</sup>

In the gapless region for  $0.4 < J_2 \leq 0.5$ , we observed the algebraic behavior of the spin correlation, which is basically consistent with the recent DMRG result by Gong *et al.*<sup>8</sup> Their estimated exponent  $\eta = 0.44$  at  $J_2 = 0.5$  is in agreement with our result  $\eta = 0.53(9)$ . As pointed out by Gong *et al.*, because the correlation length can be long, we have some uncertainty in determining whether this extended gapless region survive in the thermodynamic limit or not. If so, the power-law behavior of the spin correlation indicates that the algebraic spin liquid is realized as a phase in this region. On the other hand, if this region shrinks to the critical point in the thermodynamic limit, the deconfined quantum criticality scenario may become relevant. In this case, our estimated exponents at the transition points ( $\eta \simeq 0.0$  at  $J_2 = 0.4$  and  $\eta = 0.53(9)$  at  $J_2 = 0.5$ ) give the lower and upper bound of  $\eta$ , which does not conflict  $\eta \simeq 0.27$  obtained in the  $J$ - $Q$  model on the square lattice.<sup>27</sup> However, the size extrapolations of the staggered as well as VBC order parameters shown in Figs. 4 and 10 strongly suggest that this possibility is not plausible unless an unknown crossover occurs at larger sizes beyond the present calculation.

The existence of the gapped phase for  $0.5 < J_2 \leq 0.6$  contradicts the VMC calculation by Hu *et al.*<sup>6</sup> They calculated the energy gap between the ground state and the triplet state at  $\mathbf{K} = (\pi, 0)$  using the VMC method with the Lanczos technique and reported that this gap closes for  $J_2 > 0.48$ . We point out that, since they did not use the quantum number projection technique, the possibility that their excited states are contaminated by the ground state can not be excluded. This causes an underestimate of the energy gap after the Lanczos steps. In addition, they did not consider the possibility of the scaling form (9).

## 5. Conclusions

We have calculated the ground and excited states of the spin  $1/2$   $J_1$ - $J_2$  Heisenberg model on the square lattice by the mVMC method with high accuracy. We emphasize that, in the present study, the competing phases and their fluctuations can be represented by a unified framework and the same form of the variational wave function (2). The quantum-number projection technique has allowed us to determine the total momentum and the point group symmetry for the ground state and excitation structure. We obtained that the ground states do not have a magnetic order for  $0.4 < J_2 \leq 0.6$ . By a careful analysis of the triplet gap and the VBC order parameter, we have found a gapped phase with the VBC order for  $0.5 < J_2 \leq 0.6$ . From the excitation spectra, we conclude that the VBC order is likely to have the columnar symmetry, while it does not completely exclude the possibility of the plaquette order. On the other hand, our data support the existence of a gapless spin liquid phase for  $0.4 < J_2 \leq 0.5$ . We have also observed an algebraic behavior of the spin-spin correlation function, which indicates realization of the algebraic spin-liquid state in this region.

In this paper, while we focus on a spin system, the mVMC method is able to manage itinerant electron systems. The Hubbard model with the next-neighbor hopping term connects to the  $J_1$ - $J_2$  Heisenberg model in the limit of large Coulomb repulsion. It would be intriguing to investigate in the future study how the nature of the spin liquid becomes modified in the presence of charge fluctuations.

## Acknowledgments

The mVMC codes used for the present computation are based on that first developed by Daisuke Tahara. S.M. thanks Takahiro Misawa for fruitful discussions. This work is financially supported by MEXT HPCI Strategic Programs for Innovative Research (SPIRE) and Computational Materials Science Initiative (CMSI). Numerical calculation was partly carried out at K computer at RIKEN Advanced Institute for Computational Science (AICS) under grant number hp120043, hp120283, hp130007 and hp140215. Numerical calculation was partly carried out at the Supercomputer Center, Institute for Solid State Physics, Univ. of Tokyo. This work was also supported by Grant-in-Aid for Scientific Research (No. 22104010 and No. 22340090) from MEXT, Japan.

## Appendix: Update technique of Pfaffian

The inner product between the pair wave function and the real-space electron configuration is given as a Pfaffian of a skew-symmetric matrix. The update technique of Pfaffian for one-electron hopping is derived based on the Cayley's identity.<sup>15,28</sup> However, in a spin model, we need to generate electron configurations by two-electron exchange processes. In this appendix, we generalize the update technique for  $m$ -electron move with an arbitrary number  $m$ .

First, we summarize the definition and some properties of Pfaffian. A  $2n \times 2n$  skew-symmetric matrix  $A = [a_{ij}]$  satisfies  $A^T = -A$  ( $a_{ij} = -a_{ji}$ ), where  $A^T$  denotes the transposed matrix of  $A$ . The Pfaffian of  $A$  is defined as the antisymmetrized product

$$\text{Pf } A \equiv \mathcal{A}[a_{12}a_{34} \cdots a_{2n-1,2n}] = \sum_{\alpha} \text{sgn}(\alpha) \prod_{k=1}^n a_{i_k, j_k}, \quad (\text{A.1})$$

where the sum runs over all the pair partitions  $\alpha = \{(i_1, j_1), \cdots (i_n, j_n)\}$  with  $i_k < i_{k+1}$  and  $i_k < j_k$ . Here,  $\text{sgn}(\alpha)$  stands for the parity of the permutation corresponding to the partition  $\alpha$ . The Pfaffian satisfies the following relations,

$$\text{Pf} \begin{bmatrix} A & 0 \\ 0 & A' \end{bmatrix} = \text{Pf } A \times \text{Pf } A', \quad (\text{A.2})$$

$$\text{Pf}[BAB^T] = \det B \times \text{Pf } A, \quad (\text{A.3})$$

where  $B$  is a  $2n \times 2n$  arbitrary matrix.

Our update technique is based on the following identities:

$$\text{Pf}[A + BCB^T] = \text{Pf } A \times \frac{\text{Pf}[C^{-1} + B^T A^{-1} B]}{\text{Pf}[C^{-1}]} \quad (\text{A.4})$$

$$(A + BCB^T)^{-1} = A^{-1} - A^{-1}B(C^{-1} + B^T A^{-1} B)^{-1}B^T A^{-1}, \quad (\text{A.5})$$

where we assume  $A$ ,  $B$ , and  $C$  is a  $2n \times 2n$  invertible skew-symmetric matrix, a  $2n \times 2m$  real matrix, and a  $2m \times 2m$  invertible skew-symmetric matrix, respectively. The former identity is a Pfaffian version of the matrix determinant lemma. The more general formula of the latter is known as the Woodbury matrix identity. The proof of these formulae is shown later.

To derive the update technique, we focus on a spin-less fermion system for simplicity. The generalization to spinful electron systems is straightforward. The pair wave function

with  $2n$  fermions has a form

$$|\phi\rangle = \left( \sum_{r,r'} f_{r,r'} c_r^\dagger c_{r'}^\dagger \right)^n |0\rangle, \quad (\text{A}\cdot 6)$$

and the real-space electron configuration is

$$|x\rangle = c_{r_1}^\dagger c_{r_2}^\dagger \cdots c_{r_{2n}}^\dagger |0\rangle, \quad (\text{A}\cdot 7)$$

where  $r_i$  denotes the position of the  $i$ -th electron. The commutation relation of fermion operators yields

$$\langle x|\phi\rangle = n! \text{Pf } A, \quad (\text{A}\cdot 8)$$

where  $A$  is a  $2n \times 2n$  skew-symmetric matrix with the element  $a_{ij} \equiv f_{r_i, r_j} - f_{r_j, r_i}$ .

Suppose that  $m$  electrons with indices  $\alpha_k$  ( $k = 1, 2, \dots, m$ ) in the electron configuration  $|x\rangle$  change their positions from  $r_{\alpha_k}$  to  $r'_{\alpha_k}$ . Accordingly the inner product between the updated electron configuration  $|x'\rangle$  and the pair wave function is proportional to a Pfaffian of a new skew-symmetric matrix denoted by  $D$ . The matrix  $D = [d_{ij}]$  differs from  $A$  only in the  $\alpha_k$ -th rows and columns. We assume matrices  $B$  and  $C$  have the form as,

$$B = \begin{bmatrix} U & V \end{bmatrix}, \quad C = \begin{bmatrix} 0 & I \\ -I & W \end{bmatrix}, \quad (\text{A}\cdot 9)$$

where  $U$ ,  $V$  are  $2n \times m$  matrices and  $W$  is a  $m \times m$  skew-symmetric matrix. If we set elements of  $U$ ,  $V$ , and  $W$  as

$$U_{ik} = d_{i, \alpha_k} - a_{i, \alpha_k} \quad (\text{A}\cdot 10)$$

$$V_{ik} = \delta_{i, \alpha_k} \quad (\text{A}\cdot 11)$$

$$W_{kl} = -d_{\alpha_k, \alpha_l} + a_{\alpha_k, \alpha_l}, \quad (\text{A}\cdot 12)$$

the desired relation  $A + BCB^T = D$  is obtained. The matrix  $W$  is necessary to reduce double counting at  $(i, j) = (\alpha_k, \alpha_l)$ . We note that

$$C^{-1} = \begin{bmatrix} W & -I \\ I & 0 \end{bmatrix}, \quad (\text{A}\cdot 13)$$

and  $\text{Pf}[C^{-1}] = (-1)^{m(m+1)/2}$ .

The heaviest part of our update technique is the calculation of  $B^T A^{-1} B$  when  $m$  is  $O(1)$ . Thus, if we store the inverse matrix of  $A$ , computational cost is  $O(n^2)$  while the direct calculation of Pfaffian and inverse matrix costs  $O(n^3)$  operations.

Finally we prove two identities (A.2) and (A.3). It is easy by using the LDU decomposition of a block matrix,

$$\begin{bmatrix} A & B \\ -B^T & C^{-1} \end{bmatrix} = \begin{bmatrix} I & 0 \\ (A^{-1}B)^T & I \end{bmatrix} \begin{bmatrix} A & 0 \\ 0 & C^{-1} + B^T A^{-1} B \end{bmatrix} \begin{bmatrix} I & A^{-1}B \\ 0 & I \end{bmatrix}, \quad (\text{A.14})$$

and the UDL decomposition,

$$\begin{bmatrix} A & B \\ -B^T & C^{-1} \end{bmatrix} = \begin{bmatrix} I & BC \\ 0 & I \end{bmatrix} \begin{bmatrix} A + BCB^T & 0 \\ 0 & C^{-1} \end{bmatrix} \begin{bmatrix} I & 0 \\ (BC)^T & I \end{bmatrix}. \quad (\text{A.15})$$

The both decompositions are confirmed by direct calculations of the right-hand side. We point out that the inverse matrix of  $A$  is also skew-symmetric and  $(A^{-1}B)^T = -B^T A^{-1}$ . Equation (A.4) is derived by taking the Pfaffian of Eqs. (A.14) and (A.15) and using properties of Pfaffian (A.2) and (A.3). If we take inverse of Eqs. (A.14) and (A.15) and compare their block elements, we obtain Eq. (A.5).

## References

- 1) E. Dagotto and A. Moreo, Phys. Rev. Lett. **63**, 2148 (1989).
- 2) D. Poilblanc, E. Gagliano, S. Bacci, and E. Dagotto, Phys. Rev. B **43**, 10970 (1991).
- 3) L. Capriotti and S. Sorella, Phys. Rev. Lett. **84**, 3173 (2000).
- 4) L. Capriotti, F. Becca, A. Parola, and S. Sorella, Phys. Rev. Lett. **87**, 097201 (2001).
- 5) T. Li, F. Becca, W. Hu, and S. Sorella, Phys. Rev. B **86**, 075111 (2012).
- 6) W.-J. Hu, F. Becca, A. Parola, and S. Sorella, Phys. Rev. B **88**, 060402 (2013).
- 7) H.-C. Jiang, H. Yao, and L. Balents, Phys. Rev. B **86**, 024424 (2012).
- 8) S.-S. Gong, W. Zhu, D. N. Sheng, O. I. Motrunich, and M. P. A. Fisher, Phys. Rev. Lett. **113**, 027201 (2014).
- 9) L. Wang, Z.-C. Gu, F. Verstraete, and X.-G. Wen, arXiv:1112.3331 .
- 10) N. Read and S. Sachdev, Phys. Rev. Lett. **62**, 1694 (1989).
- 11) A. V. Chubukov and T. Jolicoeur, Phys. Rev. B **44**, 12050 (1991).
- 12) R. R. P. Singh, Z. Weihong, C. J. Hamer, and J. Oitmaa, Phys. Rev. B **60**, 7278 (1999).
- 13) M. E. Zhitomirsky and K. Ueda, Phys. Rev. B **54**, 9007 (1996).
- 14) M. Mambrini, A. Läuchli, D. Poilblanc, and F. Mila, Phys. Rev. B **74**, 144422 (2006).
- 15) D. Tahara and M. Imada, J. Phys. Soc. Jpn. **77**, 114701 (2008).
- 16) M. Wimmer, ACM Trans. Math. Softw. **38**, 30 (2012).
- 17) T. Mizusaki and M. Imada, Phys. Rev. B **69**, 125110 (2004).
- 18) T. Aimi and M. Imada, J. Phys. Soc. Jpn. **76**, 084709 (2007).
- 19) S. Sorella, Phys. Rev. B **71**, 241103 (2005).
- 20) D. A. Huse, Phys. Rev. B **37**, 2380 (1988).
- 21) S. R. White, Phys. Rev. Lett. **77**, 3633 (1996).
- 22) G. Santoro, S. Sorella, L. Guidoni, A. Parola, and E. Tosatti, Phys. Rev. Lett. **83**, 3065 (1999).
- 23) H. Neuberger and T. Ziman, Phys. Rev. B **39**, 2608 (1989).
- 24) P. Hasenfratz and F. Niedermayer, Z. Phys. B **92**, 91 (1993).



- 25) F. Becca, L. Capriotti, A. Parola, and S. Sorella, Springer Series in Solid-State Sciences **164**, 379 (2011).
- 26) R. Kaneko, S. Morita, and M. Imada, J. Phys. Soc. Jpn. **83**, 093707 (2014).
- 27) A. W. Sandvik, Phys. Rev. B **85**, 134407 (2012).
- 28) M. Bajdich, L. Mitas, L. K. Wagner, and K. E. Schmidt, Phys. Rev. B **77**, 115112 (2008).